Electronic Supplementary Material (ESI) for Journal of Materials Chemistry A.

Supporting Information

Photothermal-healing, Record Thermal Stability and Fire Safety Black Phosphorus-Boron Hybrid Nanocomposites: Mechanism of Phosphorus Fixation Effects and Charring Inspired by Cell Wall

Bin Zou, Shuilai Qiu, Yifan Zhou, Ziyan Qian, Zhoumei Xu, Jingwen Wang, Yuling Xiao, Can Liao, Wenhao Yang, Longfei Han, Fukai Chu, Lei Song, Zhou Gui*, Yuan Hu**

State Key Laboratory of Fire Science, University of Science and Technology of China, 96 Jinzhai Road, Hefei, Anhui, 230026, PR China

Contact authors: yuanhu@ustc.edu.cn; zgui@ustc.edu.cn; shuilai@ustc.edu.cn

Experimental section

Materials

Red phosphorus (99%), Tin (Sn 99.9%) powder, Tin (IV) iodide (99.9%), Isopropanol and N-methyl-2-pyrrolidone (NMP)were supplied from Aladdin Industrial Corporation (China). Boron powder (98%) was purchased from Alfa Aesar (China). Polycarbonate (PC) was purchased from Bayer (Germany).

Characterization

Atomic force microscopy (AFM) was carried out using a Dimension Icon (Bruker Nano Inc.) to characterize the size and thickness of exfoliated B nanoflakes and BP-B hybrid. Transmission electron microscopy (TEM) (JEM-2100F, Japan Electron Optics Laboratory Co., Ltd., Japan) was employed to study the morphology of BP-B. X-ray diffraction (XRD) was employed on an X-ray diffractometer (Rigaku Co., Japan). X-ray photoelectron spectroscopy (XPS) was conducted by using a VG ESCALAB MK-II electron spectrometer (V.G. Scientific Ltd., UK). Raman spectra were carried out on a Laser Micro Raman spectrometer (Jobin Yvon Co., Ltd., France) to study the structure components of BP-B and the char of PC composites. The thermal imaging camera model is Flir A655SC (FLIR, USA), and the temperature range is -20℃ to +650℃. The thermocouple is a K-type thermocouple (Φ=1mm). The mechanical properties of PC nanocomposites are tested and measured with an electronic universal testing instrument ((MTS System Co., Ltd., China)) at a speed of 5 mm/min. Thermogravimetric Mass spectrometer (TG-MS) was performed by using a Thermogravimetric analyzer of Clarus SQ 8T (PerkinElmer, USA) under a helium atmosphere, at a linear heating rate of 20 °C min^{-1} from 30 to 800 °C. The cone calorimeter test (TESTech Instrument Technology, Suzhou) was performed to study the fire performance of PC composites according to the standard of ASTM E1354/ISO

5660. Scanning electron microscopy (SEM, JEOL JSM-6700) was conducted to study micro-structures of the char residues for PC nanocomposites.

As for the photothermal healing process, dumbbell-shaped splines were cut in the width direction with scissors and placed in the original mold, and then the fractured notch was irradiated with an 808 nm laser. When the temperature of the thermocouple at the notch is greater than the melting point of 10 °C, the irradiation is stopped, and when the temperature drops to the melting point, the sample is turned over and the same operation is performed on the back. The above process was repeated three times in total, and the obtained samples were used as samples after photothermal healing for mechanical testing.

The final stable temperature Ts for photothermal conversion of composites can be estimated by (Equation (1)):

$$T_s = T_{\mathrm{h}} + \frac{(T_b - 22.5) \times 9 \times C_w}{C_c} \quad (1)$$

Where T_h is the stable temperature of the heater (PC composites), T_b is the stable temperature of the thermal storage bath, C_w is the specific heat capacity of water and C_c is the specific heat capacity of composites.

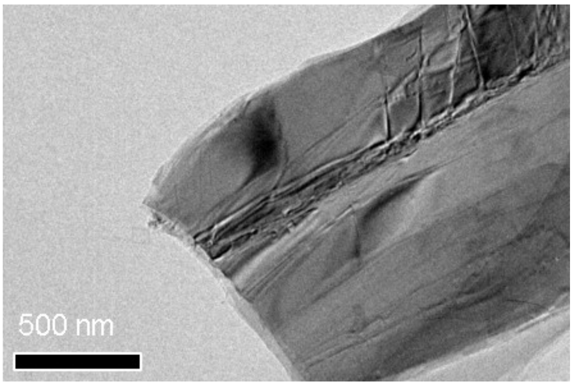

Figure S1. TEM image of BP nanoflakes.

BP nanoflakes present a flat surface and clear contours as large as several microns (Figure S1), while B nanoflakes have a stepped surface of hundreds of nanometers accompanied by tortuous edges (Figure 2a), which provides an index for the component identification of BP-B nanohybrid.

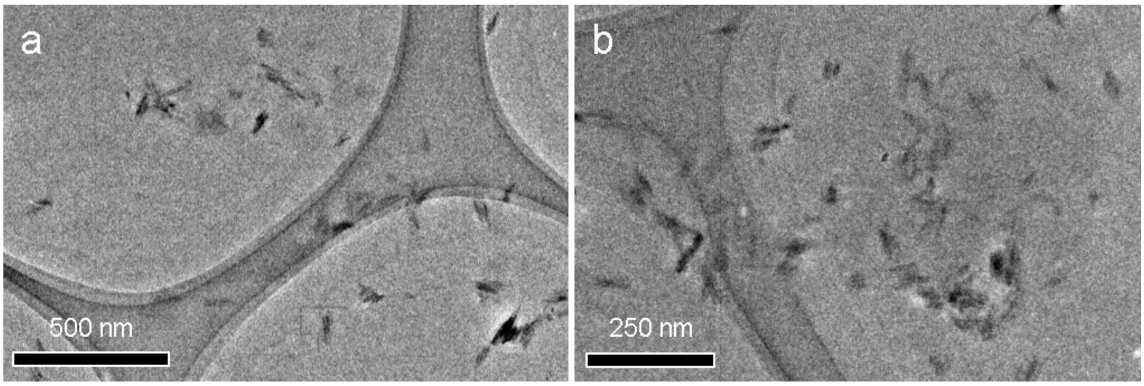

Figure S2. a) and b) TEM ultrathin section of PC/BP-$B_{1.0}$ nanocomposites at different magnifications.

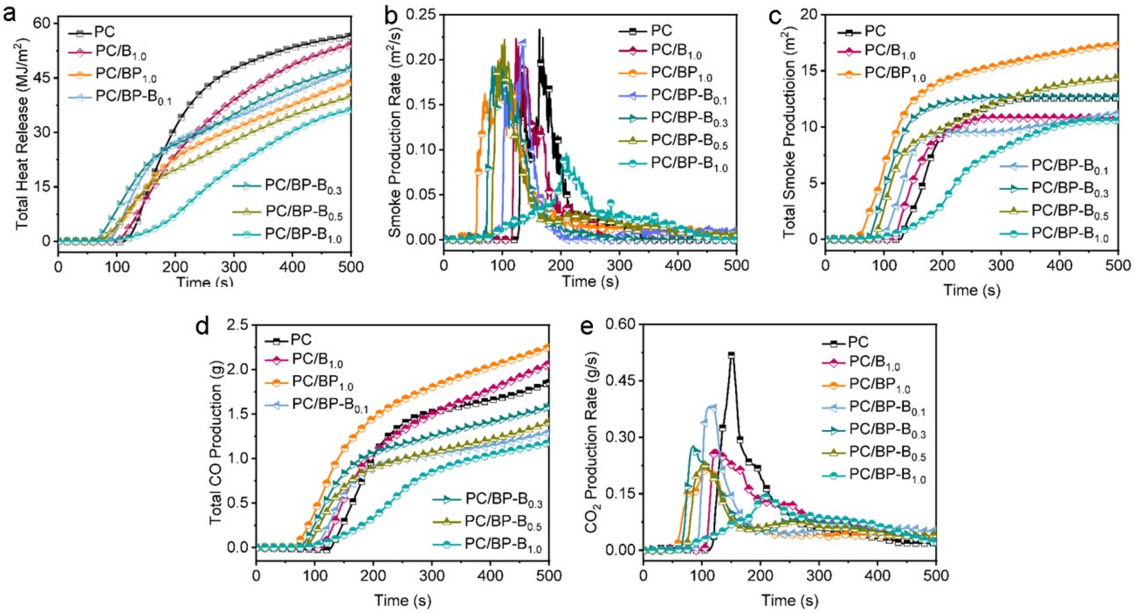

Figure S3. Smoke and gas production of PC and its nanocomposites obtained from cone calorimetry. a) Total heat release, b) Smoke production rate (SPR), c) Total smoke production (TSP), d) Total carbon monoxide production (TCOP) and e) Carbon dioxide production (CO_2).

Table S1 Cone calorimetry date of PC and its nanocomposites

Sample	PHRR[a] (kW/m^2)	ttPHRR[a] (s)	THR[a] (MJ/m^2)	PSPR[a] (m^2/s)	TSP[a] (m^2)	COP[a] (g/s)	TCOP[a] (g/m^2)	Char residue（wt %）	FGI[a] (kW/m^2·s)	LOI (%)	UL-94
PC	507.76	145	56.54	0.2337	12.56	0.0154	1.85	25.47	3.50	25.0	V-2
PC/B$_{1.0}$	281.73	154	54.16	0.2234	10.81	0.0166	2.06	23.18	1.83	28.5	V-1
PC/BP$_{1.0}$	252.10	134	43.73	0.2010	17.29	0.0163	2.25	39.35	1.88	30.5	V-0
PC/BP-B$_{0.1}$	387.12	116	47.52	0.2185	11.19	0.0144	1.29	31.15	3.34	27.5	V-1
PC/BP-B$_{0.3}$	278.24	96	47.79	0.2101	12.66	0.0137	1.58	33.67	2.90	29.0	V-1
PC/BP-B$_{0.5}$	223.29	116	39.88	0.2224	14.36	0.0135	1.40	38.42	1.92	31.0	V-0
PC/BP-B$_{1.0}$	149.81	217	36.17	0.0959	10.56	0.0064	1.18	45.69	0.69	33.0	V-0

[a] PHRR, TTPHRR, THR, TSP, COP, TCOP and FGI refer to peak heat release rate, time to peak heat release rate, total heat release, total smoke production, carbon monoxide production, total carbon monoxide production and fire growth index.

Table S2 PHHR performance and thermal stability of previous works.

Order	Flame retardant	Content (wt %)	$\Delta T_{-5\%}$ (°C)		ΔT_{man} (°C)		Reduction of PHRR (%)	References
			N_2	Air	N_2	Air		
1	SiPP	5	-55		20		19.7	[1]
2	PPSQ	4	0		0		61	[2]
3	OPS	6	–33		-6		51.2	[3]
4	BTPP	3			-70	-70	44.9	[4]
5	HSOBA	3	-59		-78		30.2	[5]
6	PPPO	6		–22	-67	-45	34.3	[6]
7	ABDPP	5	-26		-14		46.2	[7]
8	TCTP	4	-20	-9	6	3	1.8	[8]
9	AS_3	0.1	-17		-6		20.3	[9]
10	CPCn	4	10	18	34	21	44.2	[10]
11	DBS-LDH+BSR	10	-9		-3		28.6	[11]
12	ASN	0.1		-18		-2	2.6	[12]
13	SiO_2@DPP	0.8	-16		-5		41.5	[13]
14	TiO_2@DPP	0.1	-27		-8		34.1	[14]
15	DPOP-POSS	6	-45		-1		32.2	[15]
16	DBDPO	8	-58	13	-28	12	38.2	[16]
17	OPTS	0.1	-3		-33		47.1	[17]
18	Talcum	6.3	-14		-32		44.7	[18]
19	MVC-AlPi	10	-12		-27		39.2	[19]
20	BP-B	1.0	44.7		15.4		70.5	This work

Table S3 Elemental composition of BP-B obtained by EDS and XPS.

Element	EDS		XPS	
	Mass concentration (wt%)	Atomic concentration (%)	Mass concentration (wt%)	Atomic concentration (%)
B	12.12	28.31	12.77	29.52
P	87.88	71.69	87.23	70.48

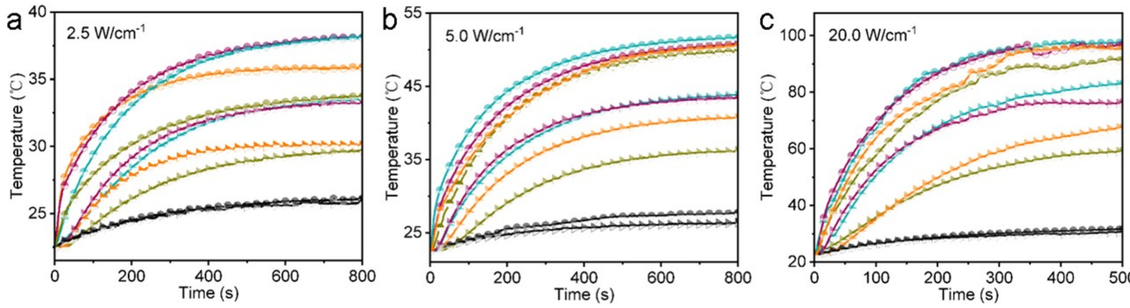

Figure S4 Heating curves of the hydrothermal measurement system of PC and its composites at different power. a) 2.5 w/cm^2, b) 5.0 w/cm^2, c) 20.0 w/cm^2.

Table S4 Characteristic parameters of linear fitting of $PC/BP_{1.0}$, $PC/B_{1.0}$, $PC/BP\text{-}B_{0.5}$ and $PC/BP\text{-}B_{1.0}$ nanocomposite photothermal systems with irradiation power.

Sample	**Intercept**		**Slope**		**R^2**	
	Heater	**Water**	**Heater**	**Water**	**Heater**	**Water**
$PC/BP_{1.0}$	9.887	6.717	3.265	1.963	0.969	0.948
$PC/B_{1.0}$	11.691	7.348	3.326	2.366	0.957	0.993
$PC/BP\text{-}B_{0.5}$	7.761	7.317	8.604	3.116	0.978	0.929
$PC/BP\text{-}B_{1.0}$	13.000	5.700	3.264	2.760	0.927	0.994

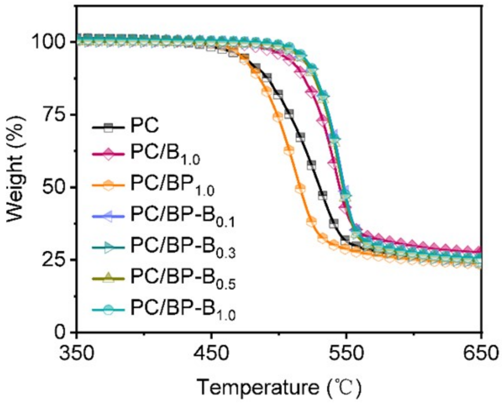

Figure S5 Thermal behavior of PC/BP, PC/B and PC/BP-B nanocomposites under nitrogen.

Table S5 Mechanical properties of PC and its nanocomposites

Sample	**Original performance**		**Photothermal healing**	
	Tensile strength (MPa)	**Elongation at break (%)**	**Tensile strength (MPa)**	**Elongation at break (%)**
PC	65.70	106.82	-	-
$PC/B_{1.0}$	65.50	43.70	64.18	29.60
$PC/BP_{1.0}$	65.67	59.63	64.59	28.06
$PC/BP\text{-}B_{0.5}$	65.43	106.94	63.74	29.13
$PC/BP\text{-}B_{1.0}$	66.31	114.81	65.85	28.59

Table S6 TGA date of PC and its nanocomposites under inert atmosphere.

Sample	**$T_{-1\%}$[a] (℃)**	**$T_{-2\%}$[a] (℃)**	**$T_{-5\%}$[a] (℃)**	**T_{max}[a] (℃)**
PC	427.69	436.81	455.71	512.38
PC/$B_{1.0}$	459.35	470.79	486.87	524.47
PC/$BP_{1.0}$	438.47	446.27	455.06	496.00
PC/BP-$B_{0.1}$	476.41	486.52	498.11	528.57
PC/BP-$B_{0.3}$	476.57	487.01	499.61	527.76
PC/BP-$B_{0.5}$	473.89	485.99	498.08	527.39
PC/BP-$B_{1.0}$	484.85	491.48	500.43	527.75

[a] $T_{-1\%}$, $T_{-2\%}$, $T_{-5\%}$ and T_{max} refer to the temperature for 1%, 2%, 5% and max rate of weight loss.

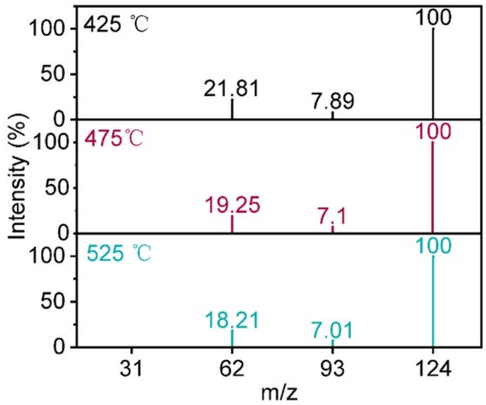

Figure S6 The mass spectra of BP pyrolytic at different temperatures.

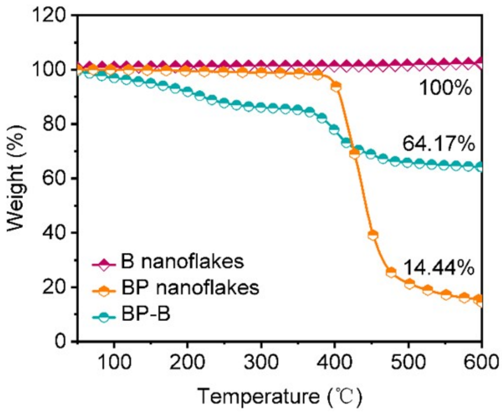

Figure S7. The thermal stability of B nanoflakes, BP nanoflakes and BP-B.

Observing the thermal weight loss behavior of B nanoflakes, BP nanoflakes and BP-B, B nanoflakes have good thermal stability with no obvious thermal weight loss occurring at 50~600°C, and BP can resist high temperatures exceeding 400°C, which indicates predominant thermal stability to adapt to the processing procedures of polymers. Pay attention to the thermal weight loss behavior of BP-B. The thermal weight loss greater than 400°C is presumed to be the thermal degradation of BP.

Without considering the limitation of oxygen, it is assumed that the P and B elements in BP-B are completely converted into BPO_4, as in Equation (2):

$$\frac{\frac{M_B}{10.81}}{\frac{M_{BP}}{30.97}} = 1:1 \quad (2)$$

Equation (3),

$$\frac{M_B}{M_{BP}} = \frac{1}{2.86} \quad (3)$$

Where M_B is the weight percentage of B in BP-B, and M_{BP} is the weight percentage of BP in BP-B.

The actual residue is 64.17%, which means the formation of heat-resistant and stable substances between the two components in the BP-B hybrid after heating.

Figure 6e shows the typical mass spectrum peaks at the maximum ion current intensity of PC and its composites. The characteristic peaks with m/z=107 are indexed to C_7H_8O, and the attached fragment peaks of phenol at m/z=94, 66 and 65. The fragments of the benzene ring are located at m/z=77, 51 and 50, which, is consistent with the structural information of PC, indicating that the main pyrolysis products of PC are aromatic compounds and hydrocarbons. Hydrocarbon is the main fuel that tends to cause thermal hazards in fires, while aromatic compound tends to condense into the particulate matter in the flue gas. Meanwhile, the conversion of phenol to stupid provides abundant OH· for the degradation process and promotes the chain reaction of the pyrolysis and combustion.

References

[1] Z. Tang, Y. Li, Y.J. Zhang, P. Jiang, Oligomeric siloxane containing triphenylphosphonium phosphate as a novel flame retardant for polycarbonate, Polym. Degrad. Stab., 97 (2012) 638-644.

[2] Y. Jiang, X. Li, R.J.J.o.a.p.s. Yang, Polycarbonate composites flame‐retarded by polyphenylsilsesquioxane of ladder structure, J. Appl. Polym. Sci., 124 (2012) 4381-4388.

[3] L. Li, X. Li, R. Yang, Mechanical, thermal properties, and flame retardancy of PC/ultrafine octaphenyl‐POSS composites, J. Appl. Polym. Sci., 124 (2012) 3807-3814.

[4] W. Zhao, B. Li, M. Xu, L. Zhang, F. Liu, L. Guan, Synthesis of a novel flame retardant containing phosphorus and sulfur and its application in polycarbonate, Polym. Eng. Sci., 52 (2012) 2327-2335.

[5] L. Ding, R. Song, B. Li, An easy‐to‐obtain silicone‐containing flame retardant and its effects on the combustion of polycarbonate, J. Appl. Polym. Sci., 126 (2012) 1489-1496.

[6] W. Zhao, B. Li, M. Xu, F. Liu, L. Guan, Synthesis of a phenylene phenyl phosphine oligomer and its flame retardancy for polycarbonate, J. Appl. Polym. Sci., 127 (2013) 2855-2866.

[7] X. Ji, N. Kong, J. Wang, W. Li, Y. Xiao, S.T. Gan, Y. Zhang, Y. Li, X. Song, Q. Xiong, A novel top‐down synthesis of ultrathin 2D boron nanosheets for multimodal imaging‐guided cancer therapy, Adv. Mater., 30 (2018) 1803031.

[8] Y. Yang, W. Kong, Y. Wang, X. Cai, Synthesis of tris (phenoxy) trifluorocyclotriphosphazenes and study of its effects on the flammable, thermal, optical, and mechanical properties of bisphenol-A polycarbonate, J. Therm. Anal. Calorim., 122 (2015) 805-816.

[9] D.Y. Zhu, J.W. Guo, J.X. Xian, S.Q. Fu, Novel sulfonate-containing halogen-free flame-retardants: Effect of ternary and quaternary sulfonates centered on adamantane on the properties of polycarbonate composites, RSC advances, 7 (2017) 39270-39278.

[10] T. Sai, S. Ran, Z. Guo, H. Yan, Y. Zhang, H. Wang, P. Song, Z. Fang, Transparent, highly thermostable and flame retardant polycarbonate enabled by rod-like phosphorous-containing metal complex aggregates, Chem. Eng. J., 409 (2021) 128223.

[11] Y. Jiang, Z. Hao, H. Luo, Z. Shao, Q. Yu, M. Sun, Y. Ke, Y. Chen, Synergistic effects of boron-doped silicone resin and a layered double hydroxide modified with sodium dodecyl benzenesulfonate for enhancing the flame retardancy of polycarbonate, Rsc Advances, 8 (2018) 11078-11086.

[12] W. Wen, J. Guo, X. Zhao, X. Li, H. Yang, J.-K. Chen, Synthesis of an Efficient S/N-Based Flame Retardant and Its Application in Polycarbonate, Polymers, 10 (2018) 441.

[13] Y.-X. Wei, C. Deng, Z.-Y. Zhao, Y.-Z. Wang, A novel organic-inorganic hybrid SiO2@ DPP for the fire retardance of polycarbonate, Polym. Degrad. Stab., 154 (2018) 177-185.

[14] Y.-X. Wei, C. Deng, H. Chen, L. Wan, W.-C. Wei, Y.-Z. Wang, Novel Core–Shell Hybrid Nanosphere towards the Mechanical Enhancement and Fire Retardance of Polycarbonate, ACS Appl. Mater. Interfaces, 10 (2018) 28036-28050.

[15] X. Wang, W. Zhang, Z. Qin, R. Yang, Optically transparent and flame-retarded polycarbonate nanocomposite based on diphenylphosphine oxide-containing polyhedral oligomeric silsesquioxanes, Compos. Part A Appl. Sci. Manuf., 117 (2019) 92-102.

[16] S. Ran, R. Ye, Y. Cai, H. Shen, Y. He, Z. Fang, Z. Guo, Synergistic flame retardant mechanism of lanthanum phenylphosphonate and decabromodiphenyl oxide in polycarbonate, Polym. Compos., 40 (2019) 986-999.

[17] Y.-X. Wei, C. Deng, W.-C. Wei, H. Chen, Y.-Z.J.A.A.N.M. Wang, Hybrid nanorods composed of titanium, silicon, and organophosphorus as additives for flame-retardant polycarbonate, ACS Appl. Nano Mater., 2 (2019) 4859-4868.

[18] Y. Qiao, Y. Wang, M. Zou, D. Xu, Y. Pan, Z. Luo, B. Wang, One-step synthesis of highly efficient oligo (phenylphosphonic dihydroxypropyl silicone oil) flame retardant for polycarbonate, Polymers, 11 (2019) 1977.

[19] L. Shao, B. Xu, W. Ma, J. Wang, Y. Liu, L. Qian, Flame retardant application of a hypophosphite/cyclotetrasiloxane bigroup compound on polycarbonate, J. Appl. Polym. Sci.,

137 (2020) 48699.